Biogenic silver nanoparticles: understanding the antimicrobial mechanism using Confocal Raman Microscopy

María Belén Estevez[1], Scott G. Mitchell[2,3], Ricardo Faccio[4*] and Silvana Alborés[1*]

[1]Área de Microbiología, Departamento de Biociencias, Facultad de Química, Universidad de la República, Montevideo (Uruguay).
[2]Instituto de Ciencia de Materiales de Aragón (ICMA), Consejo Superior de Investigaciones Científicas (CSIC)-Universidad de Zaragoza, C/ Pedro Cerbuna 12, 50009 Zaragoza (Spain).
[3]CIBER-BBN, Instituto de Salud Carlos III, Madrid (Spain)
[4]Centro NanoMat & Grupo Física, Departamento de Experimentación y Teoría de la Estructura de la Materia y sus Aplicaciones (DETEMA), Facultad de Química, Universidad de la República, Montevideo (Uruguay).

*Corresponding authors:
E-mail: salbores@fq.edu.uy; rfaccio@fq.edu.uy

Abstract

The antimicrobial properties of silver nanoparticles (AgNPs) have made them ubiquitous in a number of real-world industrial applications; however, the antimicrobial mode of action of biogenic AgNPs is not entirely understood. The use of Raman spectroscopy can provide molecular fingerprint information on various chemical and biochemical components in complex systems like microbial cultures, without the need for any complex sample pre-treatment. Consequently, the antimicrobial mechanism of AgNPs can be inferred through morphological and compositional changes of microbial cells that are monitored *via* changes in Raman band profiles. Here we show the synthesis of biogenic AgNPs using the extracellular cell-free filtrates of *Penicillium expansum*. The antimicrobial activity of the *Penicillium expansum* synthesized silver nanoparticles (hereafter PeNPs) was evaluated and the interactions between the nanoparticles and *Escherichia coli* were studied using Transmission Electron Microscopy (TEM) and Environmental Scanning Electron Microscopy (ESEM), showing the attachment of PeNPs to the surface of the bacteria and rupture of the bacterial cell membrane. Importantly, we show how Confocal Raman Microscopy can be used as an innovative approach to study the antimicrobial mechanisms, the results of which confirm that the PeNPs induce damage to bacterial and fungal cells, resulting in critical changes to polysaccharides, lipids, proteins and nucleic acids.

Keywords: biogenic nanoparticles, antimicrobial, Confocal Raman Microscopy, nanoparticle-microorganism interactions

1. Introduction

In recent years, the biological synthesis of nanoparticles, including the intracellular or extracellular production of nanoparticles by microorganisms [1; 2] has gained interest over other chemical and physical methods [3]. Extracellular biosynthesis using fungi could also make downstream processing much easier than the intracellular biosynthesis [4]. In particular, silver nanoparticles (AgNPs) have attracted considerable attention due to their applications as antimicrobial agents [5; 6]. The antimicrobial action mechanisms of AgNPs are known to be complex [7] and depend on many factors such as the physicochemical properties of the type of nanoparticle (for example, their size, shape and surface charge) or type of microorganism [8].

The use of Raman spectroscopy is an important vibrational spectroscopic tool that can provide molecular fingerprint information on various chemical and biochemical components in complex systems like microbial cultures, without any complex sample pre-treatment. Changes in cellular composition, such as proteins, lipids and nucleic acids, can be monitored using changes in Raman band profiles, which can be associated with the morphological changes of microbial cells, providing an image of the antimicrobial effect [9]. In recent times, Raman difference spectroscopy has been shown to provide molecular details on changes within *E. coli* cells caused by antibiotics, hydrogen peroxide [10; 11] or graphene oxide [9]. The objective of the present study was to produce silver nanoparticles (AgNPs) using the extracellular cell-free filtrates of *Penicillium expansum*, evaluate their antimicrobial activity and study nanoparticle-microorganism interactions. Furthermore, we propose a new approach using Confocal Raman Microscopy to study the antimicrobial mechanism of silver nanoparticles.

2. Material and Methods

2.1 Synthesis of silver nanoparticles

Strain of *Penicillium expansum* (14S) from the Cátedra de Microbiología General Collection of CCMG, Facultad de Química, Montevideo, Uruguay, was used for the nanoparticle biosynthesis.

The mycelia were grown in Potato Dextrose Agar (PDA, BD Difco) at 28 °C and two plugs of 0.9 cm in diameter were then transferred to 500 mL flasks containing 100 mL Potato Dextrose Broth (PDB, BD Difco). Fermentations were carried out at 28 °C, with agitation on an orbital shaker operating at 150 rpm for 72 hours. The biomass from cultures was harvested by filtration and then washed extensively with sterilized distilled water to remove any remaining media components. Then, synthesis of silver nanoparticles was carried out as described in Sanguiñedo *et al.*, 2018 [12]. Wet fungal mycelia were suspended in sterilized distilled water (0.1 g/mL) and incubated with agitation on an orbital shaker operating at 150 rpm. Then, the cell-free filtrate was collected by filtration of this suspension through membrane filter with 0.45 µm pore size. Finally, 50 mL of the cell-free filtrate was added to 50 mL of a silver nitrate solution. The mixture was incubated in dark. The absorbance spectrum was measured in the range of 250-800 nm and the maximum peak was determined, at different times. The reaction was stopped when there was no increase in the maximum absorption peak of silver nanoparticles. The remaining cell-free filtrate was used as control.

To evaluate the incidence of the reaction variables in the biosynthesis of the nanoparticles, the following experimental conditions were modified: incubation time of the mycelium with water, concentration of $AgNO_3$ and incubation temperature in the synthesis reaction.

After synthesis reaction, the samples were centrifuged at 10000 rpm for 10 min. The supernatant was removed and nanoparticles (PeNPs) were washed twice using sterilized distilled water, by centrifuging the nanoparticles for 5 min at 10000 rpm. The absorbance peak of the purified silver nanoparticles was measured and the concentration was estimated according to Paramelle *et al.* [13].

2.2 Characterization of silver nanoparticles

2.2.1 UV-Vis spectroscopy

The absorbance spectrum was measured in the range of 250-800 nm as evidence for silver nanoparticles formation.

2.2.2 Small Angle X-ray Scattering (SAXS)

For the Small Angle X-ray Scattering measurements, an X-Ray Powder Diffractometer, Rigaku Ultima IV model, using radiation CuK_α = 1.5418 Å was used. The measurements were made at low angle, in Bragg-Brentano geometry, applying an offset of 0.2 $Å^{-1}$ on nanoparticle deposits on silicon substrate. The measurement ranges of q = 0.05 $Å^{-1}$ to 1.50 $Å^{-1}$.

2.2.3 Dynamic Light Scattering (DLS) and ζ-potential

The hydrodynamic diameter and the ζ-potential of the nanoparticles were determined by Dynamic Light Scattering (DLS) utilizing a Malvern Instruments Zetasizer. Samples were prepared at pH 6, in Milli-Q water. For DLS determination, each sample was measured at 25 °C, 10 times, combining 5 runs per measurement. In the case of ζ-potential,

each sample was measured at 25 °C, three times, combining 10 runs per measurement. Results were treated using the Malvern software Zetasizer.

2.2.4 Confocal Raman Microscopy

An aliquot of PeNPs was deposited on an aluminum support and dried at room temperature for a further analysis by Confocal Raman Microscopy. The measurements were made on an Alpha 300 RA WITec Raman Microscope using a λ=532 nm excitation laser and focused through a 100X objective.

2.2.5 Colloidal stability assays

The nanoparticles colloidal stability was studied at different pH (3 -10) and ionic strength (10-500 mM NaCl) conditions by the measurement of the absorbance spectrum.

2.3 Antimicrobial activity of PeNPs against E. coli

2.3.1 Resazurin cell viability assays

Cell viability was analyzed using a Resazurin (7-Hydroxy-3H-phenoxazin-3-one 10-oxide) assay in a 96-well plate. A bacterial inoculum ($1x10^6$ CFU/mL) of *E. coli* DH5α in LB media was supplemented with different concentrations of PeNPs and a blank sample (bacteria without PeNPs) was also included in the assay as negative control. Once the microbial cultures had been grown for a total of 24 h, 30 µL of 0.1 mg/mL Resazurin in LB media was added to each well and incubated in the dark at 37 °C for 1 h under stirring.

2.3.2 Environmental Scanning Electron Microscopy (ESEM)

Bacterial cells were incubated with PeNPs (0.11 nM and 0.15 nM), in the same way as in the Resazurin assay. Then, three wells of 200 µL each were mixed into an Eppendorf and centrifuged at 1400 rpm (300 G) for 10 minutes. The supernatant was removed and the pellet was resuspended into 1.5 mL of 2.5 % glutaraldehyde in phosphate buffer 10 mM pH 7.2 for fixation of the cells. The solutions were left for 2 hours in the wheel. Afterwards, the cells were washed once with 1.5 mL of sterile PBS and three times with sterile distilled water to remove glutaraldehyde. Finally, the pellets were resuspended in 200 µL of sterile MilliQ water. Data were collected on a Quanta FEG-250 (FEI Company) field emission SEM for high-resolution imaging working in ESEM mode using a GSED detector under high relative humidity conditions.

2.3.3 Transmission Electron Microscopy (TEM)

Samples were prepared in the same way as in the ESEM assay, including the PeNPs concentrations. After de pellets were resuspended in sterile distilled water, 4 µL of the sample was deposited onto a carbon-coated copper grid (Cu200 mesh) and left to dry in air for several hours at room temperature. TEM analysis was carried out in a TECNAI T20 electron microscope (FEI) working at 60 kV.

2.4 Antimicrobial properties of PeNPs using Confocal Raman Microscopy

2.4.1 Antimicrobial activity

Minimum inhibitory concentration (MIC) of the nanoparticles was determined by the microdilution technique according to the Clinical and Laboratory Standards Institute (CLSI, 2012), against the following microorganisms: Gram-negative *Escherichia coli ATCC 25922*, Gram positive *Staphylococcus aureus ATCC 6538*, and *Candida albicans ATCC 101231*. MIC analyses were carried out in a 96-well plate (sterilized, 300 µL capacity, MicroWell, NUNC, Thermo-FisherScientific, Waltham, MA). The initial solutions of the nanoparticles were prepared in water and further serial dilutions were performed. The MIC was determined as the lowest silver nanoparticles concentration (antimicrobial agent) that inhibited the visible growth of a microorganism after 24 h incubation.

2.4.2 Microorganism-nanoparticle interactions by Confocal Raman Microscopy.

Studies of the phenotypic profile of microbial cells before and after treatment with silver nanoparticles were carried out using Confocal Raman Microscopy according to the methodology described for antibiotics [14]. The cell suspensions were deposited on an aluminum support and dried at room temperature. The measurements were made using a 532 nm laser focused through a 100 X objective. The data processing and statistical analysis was performed by principal component analysis (PCA) using a script to be executed with the MATLAB software. The changes obtained in the Raman spectra (phenotypic profile) of the cells treated with the nanoparticles were evaluated by comparing them with those of the untreated cells (control).

3. Results

3.1 Synthesis of silver nanoparticles (PeNPs) using Penicillium expansum

Penicillium expansum synthesized silver nanoparticles (hereafter PeNPs) were synthesized by incubating an aqueous cell-free filtrate with silver nitrate solution in the dark. A color change in the reaction mixtures, characterised by the appearance of absorption bands between 400 and 450 nm, were indicative of silver plasmon resonances associated with the production of AgNPs (Fig. 1b). No color change was

observed in the cell-free supernatant alone used as control (Fig. 1a). The spectroscopic signature associated with the biosynthesis of PeNPs (plasmon band at 440 nm) is shown in Fig. 1c.

The samples were centrifuged and the nanoparticles in the pellet were washed with water to remove unwanted reagents. After centrifugation, UV-vis spectroscopy was used to determine the stability of the PeNPs, which displayed an absorption band at 439 nm corresponding to the resonance bands of the PeNPs (Fig. 2).

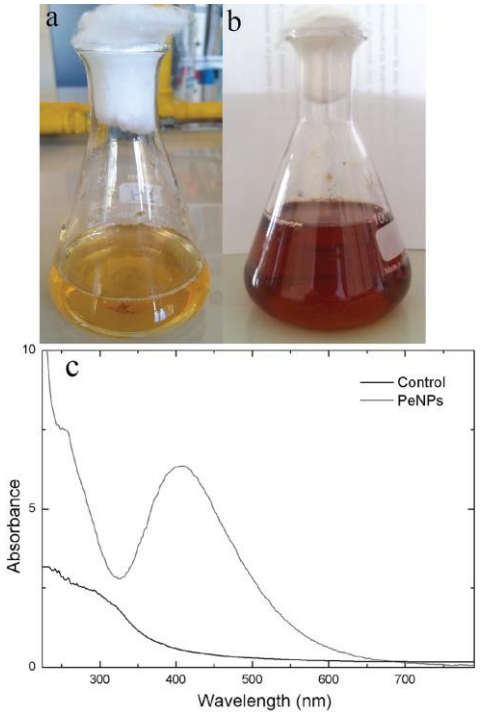

Fig. 1 Color change obtained for silver nanoparticles synthesized a) control, b) AgNPs and c) UV-Vis absorption spectra, after 24 h of reaction.

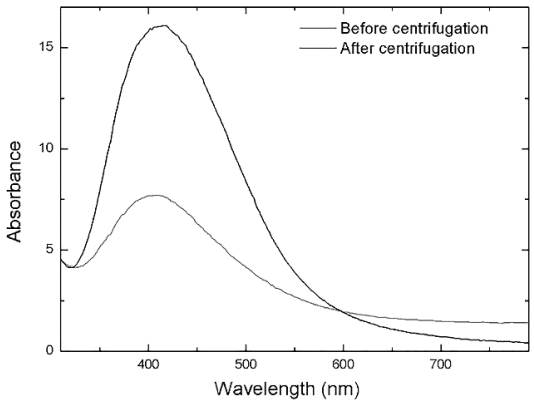

Fig. 2 UV-visible absorption spectra (before and after centrifugation) showing the plasmon resonance band of the PeNPs at 440 nm.

3.2 Evaluation of the reaction conditions in the biosynthesis of PeNPs

The $AgNO_3$ concentration, the reaction temperature and the incubation time of the mycelium with water were evaluated. 5 mM $AgNO_3$ was found to be the concentration that gave the highest yield for the nanoparticle synthesis (Fig. 3a). This concentration was selected for all subsequent biosyntheses. Moreover, results indicated that the biosynthesis reaction allowing greatest nanoparticle production in the shortest time was at 37 °C (Fig. 3b). Fig. 3c shows the evolution of silver nanoparticle synthesis over time (by measuring absorbance at 440 nm) at different incubation times. The highest biosynthesis yield of PeNPs was obtained by incubating the mycelium with water for 72 hours at 37 °C.

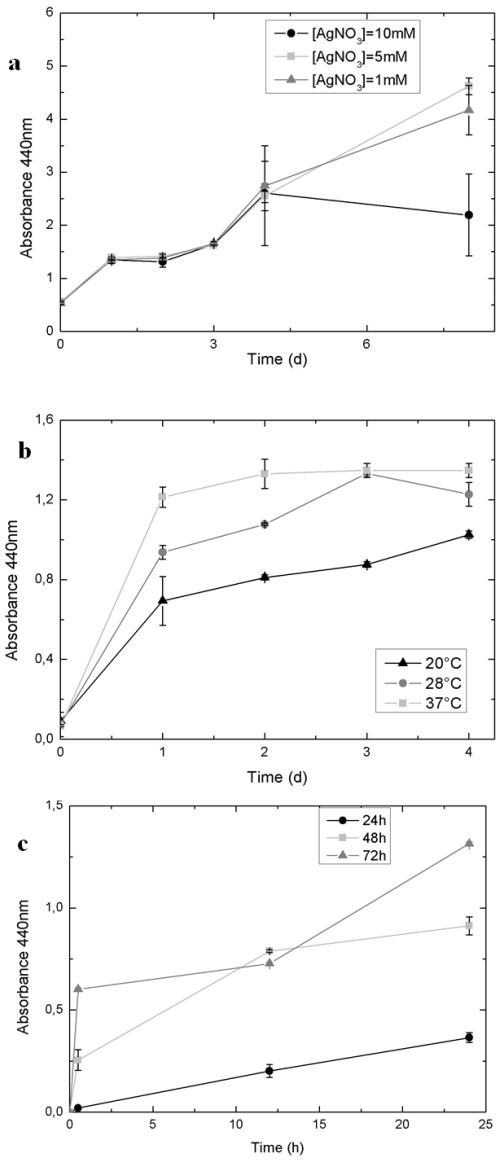

Fig. 3 Effect of different reaction conditions on the synthesis

of nanoparticles (measured by absorbance at 440 nm) over time (error bars indicate the standard deviation). a: different concentrations of silver nitrate, b: different reaction temperatures, c: different incubation times of the mycelium with water.

3.3 Characterization of PeNPs

3.3.1 DLS and SAXS

DLS characterization of the PeNPs (Fig. 4a) showed a single nanoparticle population with a hydrodynamic diameter of *ca.* 15 nm (see Online Resource 1). According to the Small Angle X-Ray Scattering measurements, the curve was fitted with a two-size-distribution model, corresponding to two-correlation lengths: one at 16 nm and another at 40 nm, the nanoparticle diameter and the distance between nanoparticles, respectively (Fig. 4b). These differences arise on the preparation of the samples, since DLS is obtained in solution, while SAXS is applied on a dried deposit from the nanoparticle solution. It is likely that during the drying process, the proximity effects of the PeNPs contributed to the second peak in the SAXS measurements.

3.3.2 ζ-potential

The stability of the PeNPs were evaluated by ζ-potential, which corresponded to -18.5 mV, indicating a relatively stable colloidal charge (see Online Resource 1)

3.3.3 Confocal Raman Microscopy

In order to further characterize the synthetized nanoparticles, Confocal Raman Microscopy was used to obtain more information about the nature of the surface functional groups capping the PeNPs. The presence of the band positioned at 230 cm^{-1} can be attributed to the Ag-N stretching mode, which may originate from the fungal extract, providing the nitrogen atoms that will finally take part of the capping of the silver nanoparticle. Additionally, the bands positioned at 1320 and 1586 cm^{-1} could be attributed to the D- and G-band of a carbonaceous component (Fig. 5).

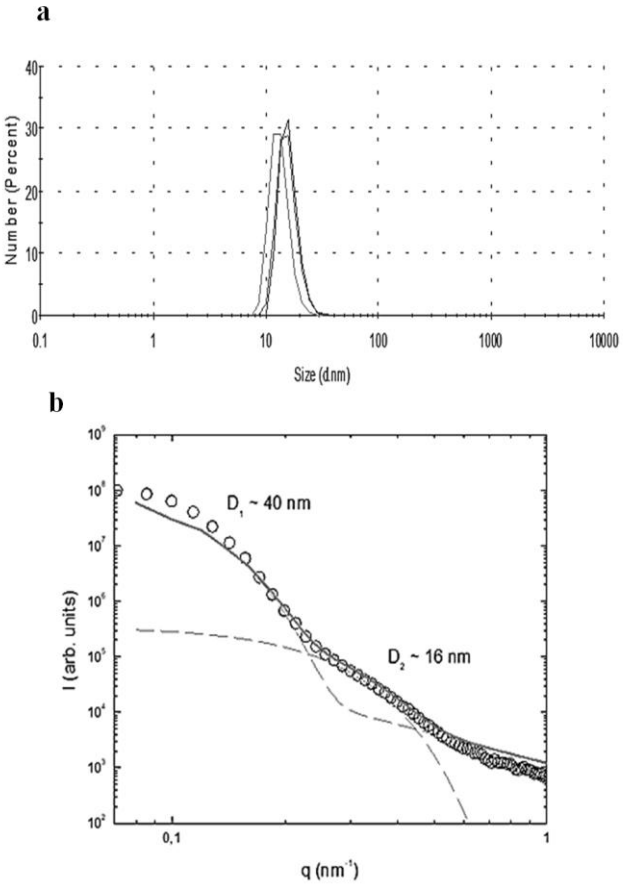

Fig. 4 (a) DLS measurement indicating monodisperse nanoparticles of *ca.* 15 nm diameter in solution and (b) the SAXS curve showing two characteristic correlated distances.

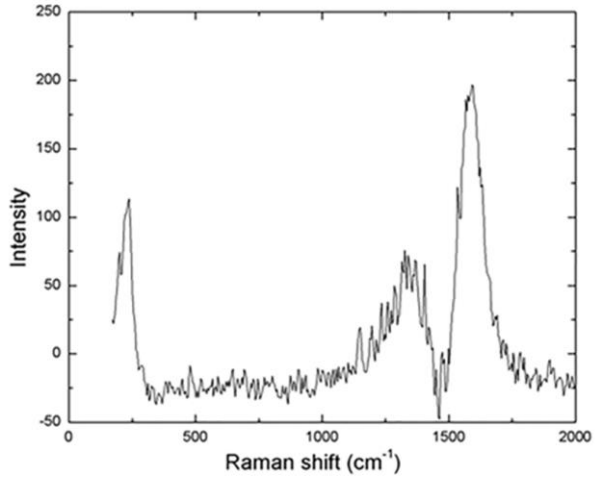

Raman Shift (cm^{-1})	Raman Assignment
219 [1]	Ag-N / Ag-O stretching
1320 [2]	D-band graphitic
1586 [2]	G-band graphitic

Fig. 5 Raman spectrum and assignment table for PeNPs.

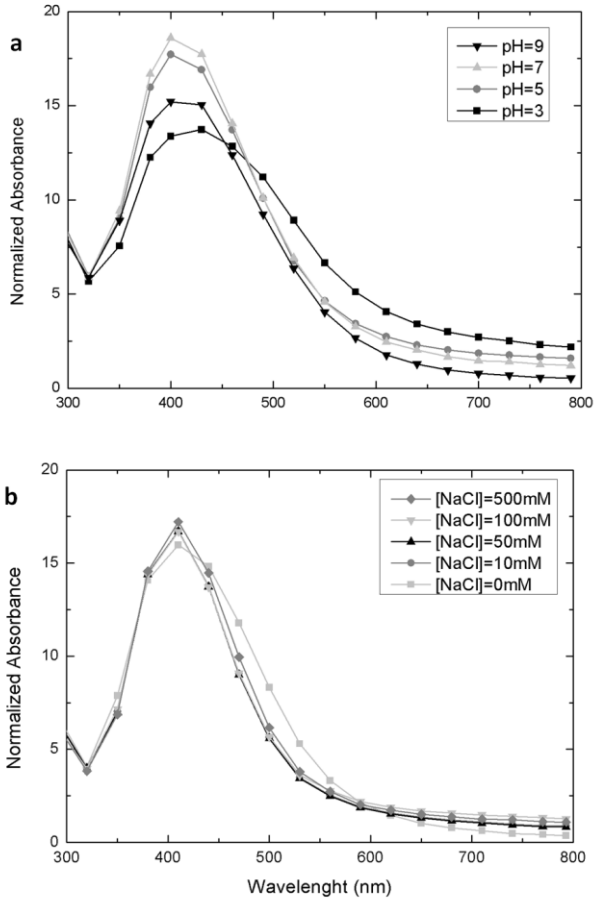

Fig. 6 Stability of PeNPs at different pH (a) and ionic strength (b).

3.3.4 Colloidal stability assays

In order to further evaluate the colloidal stability of PeNPs, we analyzed the shift in wavelength (nm) of the colloidal suspension at different pH (3-9) and ionic strength ([NaCl] = 10-500 mM). According to the results, no relevant changes occurred, thus demonstrating that the PeNPs were stable over relatively broad range of pH and conditions of onic strength (Fig. 6).

3.4 Antimicrobial activity of PeNPs against E. coli

Cell viability assays showed that the Minimum Bactericidal Concentration (MBC) was 0.22 nM. TEM and ESEM analyses where carried out to evaluate the interaction of the PeNPs with the bacteria. Sub-MBCs of 0.11 nM and 0.15 nM were used.

ESEM images in Fig. 7 show damage to the cell membrane integrity of E. coli due to the presence of PeNPs (Fig. 7c-7f), when compared with the control (Fig. 7a and 7b). This loss of the cell membrane integrity increases with PeNP concentration (Fig. 7e and 7f). Also, at both concentrations, some bacteria liberate cytoplasmic components (Fig. 7d and 7f, indicated by arrows) as a result of the interaction with the PeNPs, may be due to the generation of pores on the cell wall (see Fig. 7c).

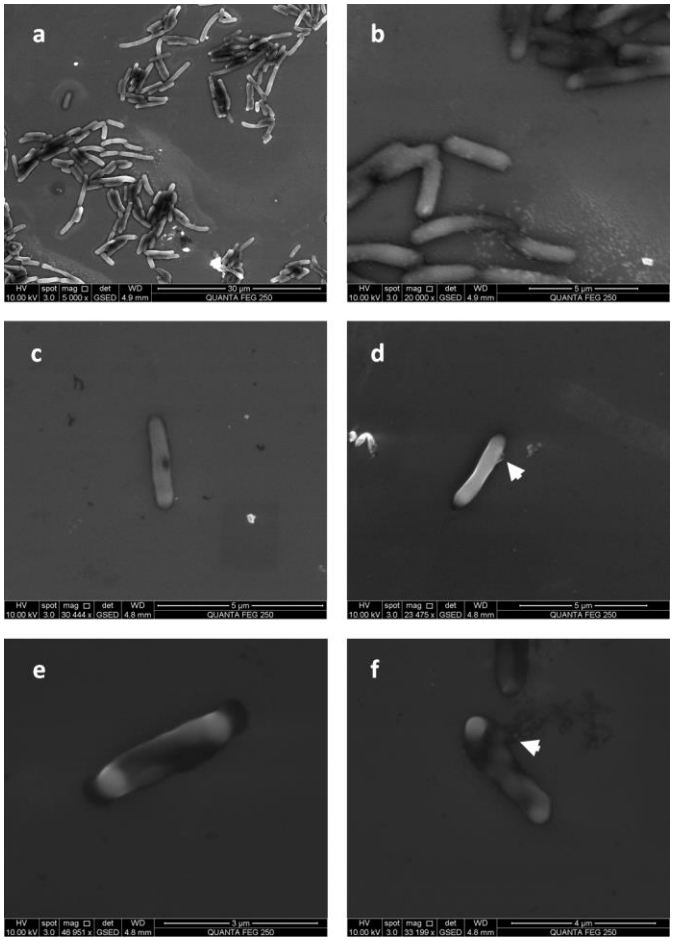

Fig. 7 ESEM images of the interaction between *E. coli* and PeNPs. a,b: control, c-f: *E. coli* with a solution of PeNPs (concentrations: c-d 0.11 nM and e-f 0.15 nM).

Damage to the cell membrane at higher PeNP concentration can be also seen in the TEM images (Fig. 8e and 8f). Furthermore, at the lowest PeNP concentration (Fig. 8c and 8d), TEM shows the nanoparticles aggregating on the surface of the bacteria, generating conglomerate PeNPs.

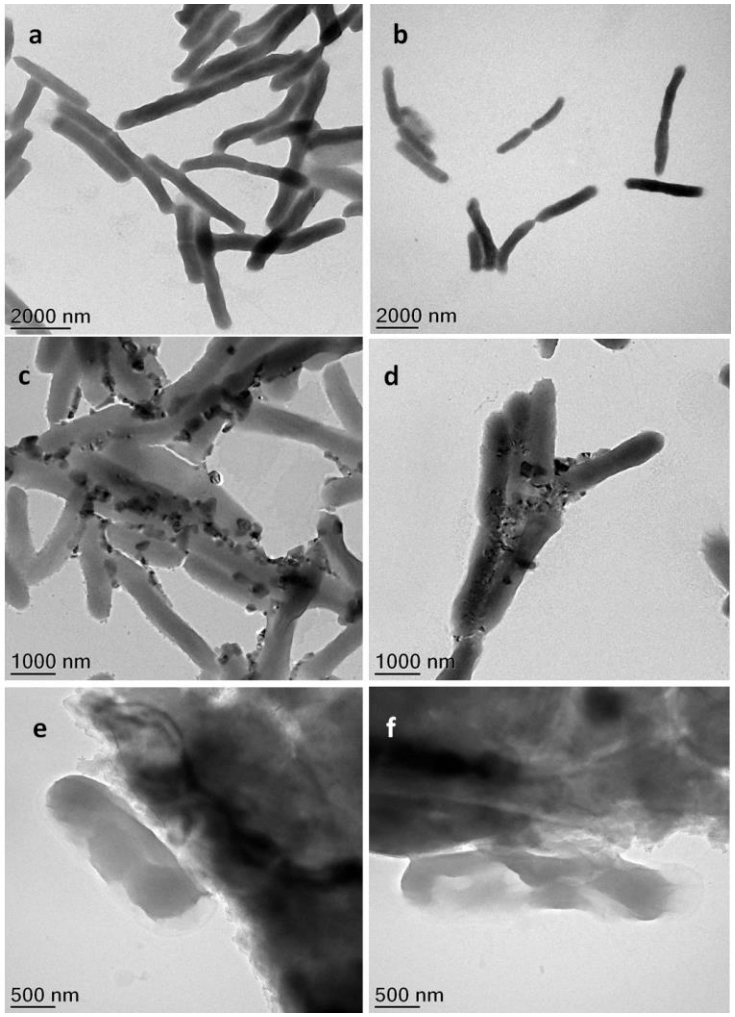

Fig. 8 TEM images of the interaction between *E. coli* and PeNPs. a,b: control, c-f: *E. coli* with a solution of PeNPs (concentrations c-d 0.11 nM and e-f 0.15 nM)

3.5 Antimicrobial properties of PeNPs using Confocal Raman Microscopy

3.5.1 Determination of the Minimum Inhibitory Concentration (MIC)

Table 1 shows the MIC values obtained for the PeNPs and the $AgNO_3$ solution against the gram-negative bacteria *Escherichia coli*, gram-positive *Staphylococcus aureus* and the yeast *Candida albicans*. All the microorganisms tested were more sensitive to the PeNPs than to $AgNO_3$ solution.

Table 1: Minimum Inhibitory Concentration (MIC) of the PeNPs and the $AgNO_3$ solution against different microorganisms.

	Escherichia coli	***Staphylococcus aureus***	***Candida albicans***
PeNPs	0.6 nM	30 pM	0.1 nM
$AgNO_3$	7.8 µM	0.6 nM	7.8 µM

3.5.2 Nanoparticle-microorganism interactions

Phenotypic changes in *E. coli*, *S. aureus* and *C. albicans* cells treated with PeNPs were analyzed by means of Confocal Raman Microscopy (Table 2). In the case of E. coli, the interaction with the nanoparticles induces an increase in the intensity of some Raman bands, while others decrease or disappear. The interaction of the nanoparticles with *S. aureus* causes a decrease in the intensity of all the bands of the Raman spectrum and for the case of *C. albicans* some bands decrease and others remain with the same intensity.

In addition, hyperspectral images were obtained in order to visualize the main characteristics of the interaction between the PeNPs and the microorganisms (see Fig. 9). These images are obtained from the combination of the bands corresponding to the C-H stretching of the microorganisms and the bands corresponding to the Ag-N stretching of the PeNPs (Raman spectra are shown in Online Resource 1).

Table 2: Raman band assignment of microbial cells, control and treated cells with PeNPs. The band assignment was made based on previous work [15].

Microorganism	**Raman Shift (cm^{-1})**	**Band Assignment**	**Effect on treated cells**
E. coli			
	624	Nucleic acids	Disappear
	810	Amino acids	Diminishes
	982	Polysaccharides	Increases
	1186	Polysaccharides	Disappear
	1308	Amino acids or nucleic acids	Increases
S. aureus			
	993	Polysaccharides	Diminishes
	1092	Polysaccharides	Diminishes
	1327	Amino acids or nucleic acids	Diminishes
	1587	Fatty acids	Diminishes
C. albicans			
	698	Nucleic acids	Diminishes
	750	Amino acids	Diminishes
	991	Polysaccharides	No changes
	1318	Amino acids or nucleic acids	No changes
	1597	Fatty acids	Diminishes

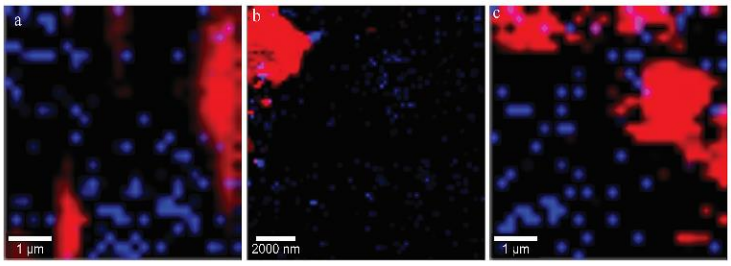

Fig. 9 Confocal Raman images obtained by combination of stretching C-H bands from microorganism (red) and the Ag-N bands assigned to the PeNPs (blue). a) *E. coli*, b) *S. aureus*, c) *C. albicans.*

4. Discussion

The silver nanoparticles synthesised with *Penicillium expansum* were stable after their purification by centrifugation [12]. The evaluation of the biosynthesis conditions of PeNPs was carried out in order to produce more stable nanoparticles in higher yield in less time, for their potential use in biotechnological applications requiring large quantities.

The size of the PeNPs was determined by Dynamic Light Scattering (DLS) and X-ray diffraction at low angles (SAXS). The average hydrodynamic diameter obtained from DLS was 14 nm. Dispersity Parameter (PDI) showed a moderate polydisperse distribution (<0.4) from DLS results. In addition, Small Angle X-ray Scattering (SAXS) analysis showed two peaks associated with populations of spherical nanoparticles. The characteristic distances obtained from the adjustment correspond to 15 nm and 40 nm (Figure 5). The first population could be attributed to the size of the single nanoparticles, while the second could correspond to a second larger population, resulting from the drying process necessary to make the preparation on silicon substrate. ζ-potential determination showed that PeNPs had net negative surface charge (-18.5 mV), indicating their stability. Nanoparticle suspensions showing ζ-potential net charges close to neutrality do not possess sufficient electrostatic repulsion to remain stable in solution.

In addition, the absorption spectrum of the nanoparticle solutions showed that the nanoparticles were stable to pH and high ionic strength. However, for the most extreme pH conditions (pH = 3 and pH = 9), a decrease in the plasmon resonance band suggested mild aggregation. Furthermore, a slight broadening of the peak is observed at pH 3 which could be attributed to the neutralization of surface charges of the PeNPs, which presented negative net charge at pH 6, resulting in their aggregation.

The characterization of the PeNPs was complemented by Confocal Raman Microscopy studies which indicated that this biological synthesis first produces AgNPs coordinated with N or O atoms, coming from the protein matrix, which enable their synthesis. In addition, the bands associated with the vibrational modes corresponding to the C-C stretching of the D- and G-bands of the carbonaceous matrix were found. These bands can be attributed to oxidized organic matter. In particular, the nature of silver nanoparticles gives rise to SERS phenomenon (Surface-Enhanced Raman Scattering), which produces a local effect. Due to this antenna and amplifier effect, it is possible to enhance the Raman signal of those molecular fragments near the surface of the nanoparticles of great importance to assess the nature of the stabilizing agent [16].

The application of biogenic PeNPs as antimicrobial agents was evaluated. The *in vitro* antimicrobial activity assays showed promising results, with MIC values lower than silver nitrate solution against bacteria and yeasts.

A first approach on the interaction between the PeNPs and *Escherichia coli* was carried out using electron microscopy techniques (TEM and ESEM). The first step in the interaction seems to be the attachment of the silver nanoparticles to the surface of the bacteria, as seen in TEM images. Thereafter, both ESEM and TEM show a decrease in the integrity of the cell membrane, probably as a consequence of the loss of cytoplasmic components due to de generation of pores on the cell, as shown in the ESEM images. In summary, the interaction of these silver nanoparticles and *Escherichia coli* seems to occur in three main stages: i) the attachment of the silver nanoparticles to the bacterial surface, ii) the generation of pores and the damage of the cell wall, and iii) the loss of cytoplasmic components and the death of the bacteria.

In order to advance in the knowledge of the antimicrobial mechanisms of action of the PeNPs against different microorganisms, Confocal Raman Microscopy studies were carried out. For this purpose, Principal Components Analysis (PCA) was used. This systematic and statistical power tool was able to demonstrate the existence of significant changes in the phenotypic profile of the microorganisms evaluated against the PeNPs (*Escherichia coli*, *Staphylococcus aureus* and *Candida albicans*). The results suggest that the AgNPs produce cellular damage, producing changes at polysaccharides, lipids, proteins and nucleic acids. Although these studies had already been addressed in studies against antibiotics, this is the first report made with biogenic silver nanoparticles, which allows to advance in the knowledge of the target sites of nanoparticles. Changes in the phenotypic profile of the Raman spectra could be associated with the generation of reactive oxygen species (ROS) and intermediate nitrogen species (RNI) since they are extremely toxic and can cause damage to proteins, lipids and DNA. Previous studies have reported that the oxidative stress would be one of the mechanisms by which the nanoparticles synthetized by *P. aeruginosa* exert their toxicity [17]. On the other hand, Raman studies on antibiotics against microorganisms showed DNA fragmentation. The decrease of the band associated with DNA in *E. coli* and *S. aureus* and the disappearance of the same Raman band for the case of *C. albicans* can be attributed to a combination of mechanisms, possibly associated with the generation of ROS, which lead to the fragmentation and death of the microbial cells [18].

5. Conclusions

Extracellular cell-free filtrates of *Penicillium expansum* were used for the biosynthesis of monodisperse 15-nm diameter silver nanoparticles (PeNPs). Here we reported the optimum biosynthesis conditions to obtain the highest production of PeNPs in the shortest time for their potential use in biotechnological applications requiring large quantities of silver nanoparticles. The size, surface charge and stabilizing agent of the PeNPs were characterized, showing that the

biogenic PeNPs were stable over a wide range of pH and ionic strength. The *in vitro* antimicrobial activity assays showed promising results for the application of biogenic nanoparticles as antimicrobial agents with MICs in the nM range. The interaction between the PeNPs and *Escherichia coli* was characterized using TEM and ESEM, showing the attachment of silver nanoparticles to the surface of the bacteria, which was accompanied by a coresponding decrease in the integrity of the cell wall. Importantly, a new approach to study the antimicrobial mechanism of biogenic silver nanoparticles, using Confocal Raman Microscopy allowed us to suggest that the damage to bacterial and fungal cells produced by the PeNPs induces changes to polysaccharides, lipids, proteins and nucleic acids.

Acknowledgements

This work was supported by the Comisión Sectorial de Investigación Científica (CSIC) y Comisión Académica de Posgrado (CAP) (Universidad de la República, Uruguay), Program for the Development of Basic Sciences (PEDECIBA-Química) and Agencia Nacional de Investigación e Innovación (ANII) -Uruguay. Authors acknowledge use of the Advanced Microscopy Laboratory at The University of Zaragoza.

References

[1] Alamri SAM, Hashem, M., Nafady, N.A., Sayed, M.A., Alshehri, A.M., Alshaboury, G. Controllable biogenic synthesis of intracellular Silver/Silver Chloride Nanoparticles by *Meyerozyma guilliermondii* KX008616. Journal of Microbiology and Biotechnology. 2018; 28(6):917.

[2] Javani S, Marín I, Amils R, Abad JP. Four psychrophilic bacteria from Antarctica extracellularly biosynthesize at low temperature highly stable silver nanoparticles with outstanding antimicrobial activity. Colloids and Surfaces A: Physicochemical and Engineering Aspects. 2015; 483:60-9.

[3] Husain S, Sardar M, Fatma T. Screening of cyanobacterial extracts for synthesis of silver nanoparticles. World Journal of Microbiology and Biotechnology. 2015;31(8):1279-83.

[4] Li G, He D, Qian Y, Guan B, Gao S, Cui Y, et al. Fungus-mediated green synthesis of silver nanoparticles using *Aspergillus terreus*. International Journal of Molecular Sciences. 2012;13(1):466-76.

[5] Sripriya J, Anandhakumar S, Achiraman S, Antony JJ, Siva D, Raichur AM. Laser receptive polyelectrolyte thin films doped with biosynthesized silver nanoparticles for antibacterial coatings and drug delivery applications. International Journal of Pharmaceutics. 2013;457(1):206-13.

[6] Mosselhy DA, El-Aziz MA, Hanna M, Ahmed MA, Husien MM, Feng Q. Comparative synthesis and antimicrobial action of silver nanoparticles and silver nitrate. Journal of Nanoparticle Research. 2015;17(12):1-10.

[7] Durán N, Durán M, de Jesus MB, Seabra AB, Fávaro WJ, Nakazato G. Silver nanoparticles: A new view on mechanistic aspects on antimicrobial activity. Nanomedicine: Nanotechnology, Biology, and Medicine. 2016;12(3):789-99.

[8] Kedziora, A, Speruda, M, Krzyzewzca, E, Rybka, J, Lukowiac, A, Bugla-Ploskonska, G. Similarities and Differences between Silver Ions and Silver in Nanoforms as Antibacterial Agents. International Journal of Molecular Science. 2018;19(2): pii: E444. doi: 10.3390/ijms19020444

[9] Nanda SS, Yi DK, Kim K. Study of antibacterial mechanism of graphene oxide using Raman spectroscopy. Scientific Reports. 2016;6.

[10] Xuan Nguyen NT, Sarter S, Hai Nguyen N, Daniel P. Detection of molecular changes induced by antibiotics in *Escherichia coli* using vibrational spectroscopy. Spectrochimica Acta - Part A: Molecular and Biomolecular Spectroscopy. 2017; 183:395-401.

[11] Carey PR, Whitmer GR, Yoon MJ, Lombardo MN, Pusztai-Carey M, Heidari-Torkabadi H, et al. Measuring Drug-Induced Changes in Metabolite Populations of Live Bacteria: Real Time Analysis by Raman Spectroscopy. Journal of Physical Chemistry B. 2018;122(24):6377-85.

[12] Sanguiñedo P, Fratila, R. M., Estevez, M. B., Martínez de la Fuente, J., Grazú, V., Alborés, S.. Extracellular Biosynthesis of Silver Nanoparticles Using Fungi and Their Antibacterial Activity. Nano Biomedicine and Engineering. 2018;10(2):156-64.

[13] Paramelle D, Sadovoy A, Gorelik S, Free P, Hobley J, Fernig DG. A rapid method to estimate the concentration of citrate capped silver nanoparticles from UV-visible light spectra. Analyst. 2014;139(19):4855-61.

[14] Athamneh AIM, Alajlouni RA, Wallace RS, Seleem MN, Sengera RS. Phenotypic profiling of antibiotic response signatures in *Escherichia coli* using raman spectroscopy. Antimicrobial Agents and Chemotherapy. 2014;58(3):1302-14.

[15] De Gelder, J, De Gussem, K, Vandenabeele, P, Moens, L. Reference database of Raman spectra of biological molecules. Journal of Raman Spectroscopy. 2007;38(9):1133-1147

[16] Joshi N, Pathak A, Upadhyaya CP, Jain N, Singh J, Prasad R. Biosynthesis of silver nanoparticles using *Carissa carandas* berries and its potential antibacterial activities. Journal of Sol-Gel Science and Technology. 2018;86(3):682-9.

[17] Quinteros MA, Cano Aristizábal V, Onnainty R, Mary VS, Theumer MG, Granero GE, Paraje MG, Páez PL. Biosynthesized silver nanoparticles: Decoding their mechanism of action in *Staphylococcus aureus* and *Escherichia coli*. International Journal of Biochemistry & Cell Biology. 2018; 104:87-93.

[18] Bernatová S, Samek O, Pilát Z, Šerý M, Ježek J, Jákl P, et al. Following the mechanisms of bacteriostatic versus bactericidal action using raman spectroscopy. Molecules. 2013;18(11):13188-99.